Hooked-End Steel Fibers Affecting Damping Ratio of Modified Self-Compacting Concrete with Rubber and Marble/Granite Additions

Amauri Ernesto Gomes , Luisa A. Gachet , Rosa Cristina C. Lintz , Mirian de L. N.M. Melo , Wislei R. Osório *

Posted Date: 17 May 2024

doi: 10.20944/preprints202405.1143.v1

Keywords: mechanical properties; self-compacting concrete; waste residues; rubber content; microstructural array; composite material.

 doi:10.20944/preprints202405.1143.v1

Article

Hooked-End Steel Fibers Affecting Damping Ratio of Modified Self-Compacting Concrete with Rubber and Marble/Granite Additions

Amauri Ernesto Gomes [1], Luisa A. Gachet [2], Rosa Cristina C. Lintz [2], Mirian de L. N. M. Melo [1] and Wislei R. Osório [2,3,*]

[1] Institute of Mechanical Engineering, Federal University of Itajubá (IEM-UNIFEI), semogiro@gmail.com ; mirianmottamelo@unifei.edu.br (M.L.N.M.M)
[2] Faculdade de Tecnologia, FT, Campus I, Universidade de Campinas/UNICAMP, 13484-332 Limeira-SP, Brazil;(L.A.G) gachet@unicamp.br; R.C.C. L) rosacclintz@ft.unicamp.br.
[3] Faculdade de Ciências Aplicadas, FCA, Centro de Pesquisa em Materiais Avançados (CPMMA), Campus II, Universidade de Campinas/UNICAMP, 13484-350 Limeira-SP, Brazil;
* Correspondence: wislei1@unicamp.br

Abstract: The aim of this investigation is focused on the effects of hooked-end steel fibers on both fresh and hardened properties of modified self-compacting concretes (SCC). For this purpose, the steel fibers are associated with other residues contents (i.e. marble, granite and rubber). This concatenated materials contents constitutes a novelty since no investigations are reported. It is found that the increase of rubber content, a better ability to absorb energy is observed. This indicates that a good alternative of structural material is provided. Fresh properties are evaluated by using flow, T_{500} time, V-funnel, J-ring methods. The mechanical behavior is evaluated in terms of compressive strength, tensile strength, static and dynamic modulus of elasticity, and damping ratio. Experimental results of the water absorption, porosity and density are also attained. It is also found that a SCC mixture containing steel fiber, marble/granite residue and rubber content is a potential mixture to be considered when in SCC designing associated with improved damping ratio. Although the rubber content decreases the mechanical behavior and slump flow, the concatenated utilization of marble/granite residues and steel fiber contents provide a slight improve in the damping result. An environmental benefit can also be associated since the cement consumption is decreased with marble additions.

Keywords: mechanical properties; self-compacting concrete; waste residues; rubber content; microstructural array; composite material

1. Introduction

Self-compacting concrete (SCC) is able to flow and consolidate due to the effect of gravity and fill dense reinforcement efficiently, without any external vibration [1-2], and has high mortar content and uses fines and additives to maintain its cohesion. Several studies are reported about SCC with marble and granite residues [3-11], SCC containing rubber [12-20] and SCC with steel fiber [21-26]. However, studies concatenating rubber, marble and granite residues (MGR) with hooked-end steel fibers are scarce. The novelty intrinsically provided in this investigation concerns to fact that a new SCC is produced. This is carried out when alternative materials with distinctive nature aspects are proposed. Marble powder wastes are a by-product of the marble industry, generated in large quantities in the process of cutting and shaping marble pieces [27]. Several researches use marble and granite waste in concrete and mortar either replacing part of the cement or sand mass or only incorporating into the mixture [28-30]. From the physical point of view, the presence of marble residues in the hardened cement paste has a filling effect and the porosity of the paste is decreased [31-34]. Marble residues are made up of inert or almost inert material [27]. Some studies show that, when marble and granite residues are incorporated into the SCC (up to 10%) and replacing the cement mass, there is no significant variation in the mechanical properties of concrete [5, 10]. When

 doi:10.20944/preprints202405.1143.v1

sand portion is replaced with ~10% wt.% granite powder, the resulting compressive strength is between 8% and 12% increased [35]. On the other hand, high volumes of incorporation of marble and granite residues, brings environmental impacts, minimizing CO_2 emissions into the atmosphere, energy consumption and natural resources [6].

Interesting properties are observed when replacing natural sand with rubber residues, such as reduction of slump-flow of SCC [12, 18], reduction of passing ability [36], reduction the concrete density [37], improvement of the energy absorption capacity of the cement composite [38] and increase in the ductility of the concrete [16]. Najim and Hall [39] and Li et al. [12] found that the damping rate increases with the addition of rubber residue in the concrete. Structural steel fibers are used in concrete as a reinforcement material to modify ductility, improving the toughness of hardened concrete. In the fresh state, steel fibers in the SCC reduce fluidity and hinder the ability to pass through mixing obstacles [40, 24]. And, in the process of casting the concrete, they influence the mechanical performance of the set according to its type, its distribution and orientation [41, 42, 43, 44].

Regarding the hardened state of the SCC reinforced with steel fibers, there is no significant change in compressive strength or in Young's modulus [22, 45-46]. Steel fibers prevent the growth of cracks in concrete and it increases the energy absorption [24, 47-48]. Fiber reinforced concrete is a composite material that has improved post-cracking behavior due to the bridge that is made between the crack faces by the fibers. Majority investigations have studied the feasibility of using alternative materials for the production of concrete.

The novelty provided in this present investigation concern to hooked-end steel fiber additions associated with rubber, marble and granite contents. The simultaneous use of these materials on the mechanical properties of SCC is scarcely reported. Additionally, it is found that the damping ratio is improved with concatenated residues contents associated with steel fiber inclusions. It is important to remark that this investigation has certain limitations. It is anchored to specific combinations of additives and their concentrations. Evidently, some other possible interactions and effects on SCC properties cannot be focused on these attained results, when broader range of construction scenarios is considered. It is remembered that another limitation concerns to the fact the attained results are laboratory-based analyses. This seems to limit the direct translation of its findings to real-world applications without comprehensive field validation. Thus, further empirical research to fully harness the benefits of the modified SCC in various environmental and operational contexts are requested.

2. Experimental Procedures

2.1. Materials

High early strength (HES) Portland cement (according ASTM C150) is used, and its physical properties and chemical composition are show in Tables 1 and 2. The fine aggregate consisted of natural quartzite sand; the coarse aggregate is of basaltic origin (Table 1). Silica fume is the mineral addition used in the SCC preparing. This material is incorporated into the mixture intending to increase the resulting strength. This due to the effects of micro filler and refinement of the pore structure and cement hydration products is recognized. Tables 1 and 2 show the physical properties and chemical composition. Marble and granite residue (MGR) is used in the production of SCC as the fine content. It is obtained in a wet condition from the ornamental stone industry, located at Limeira, SP, Brazil, and used in a dry condition. The physical properties and chemical composition of the MGR are listed in Tables 1 and 2. The Laser Method (ISO 13320:2009) is applied in order to the granulometric characterization be carried out. The rubber waste tires are also used, as depicted Figure 1.

The physical properties and the chemical elements are demonstrated into Tables 1 and 2. The drinkable tap water is used in molding and curing stages. A polycarboxylate ether based superplasticizer (SP) is used, as shown Table 1.

 doi:10.20944/preprints202405.1143.v1

Hooked-end steel fibers (HESF) designated as Dramix® RC65/35B are used, as depicted Figure 2. The tensile strength of the steel fibers is 1,345 (±50) N/mm², length is 35 (±1) mm, diameter is 0.55 (±0.05) mm, form factor is 65 and modulus of elasticity is 200,000 N/mm².

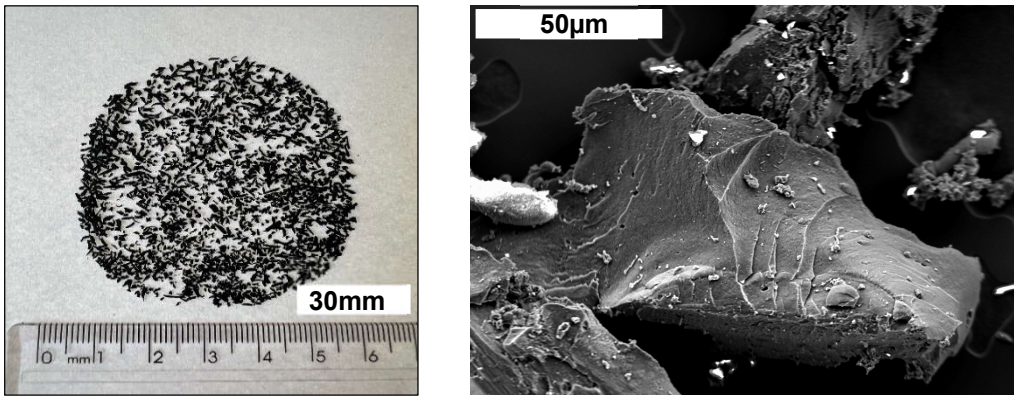

(**a**) (**b**)

Figure 1. Rubber residues **(a)** macroscopic scale and **(b)** Secondary electron microscope (SEM) image by using secondary electron (SE) technique to characterize rubber particle.

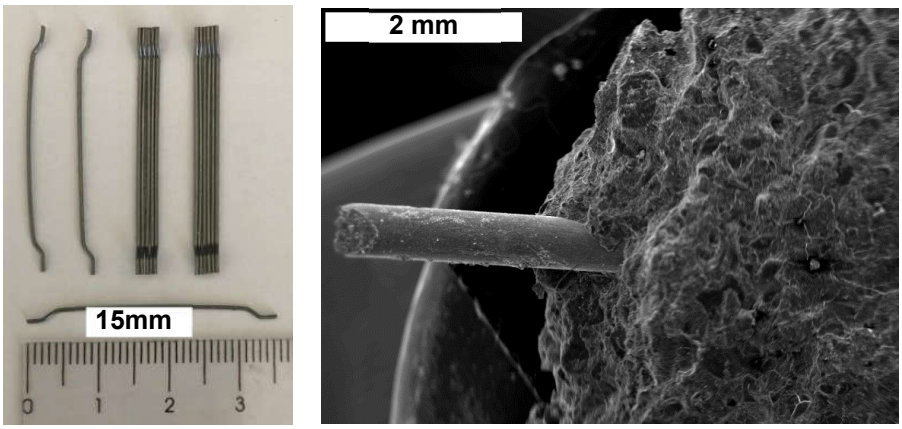

(**a**) (**b**)

Figure 2. (a) Hooked-end steel fibers (HESF) designated as Dramix® RC65/35B and **(b)** typical SEM/SE image evidencing steel fiber reinforced concrete sample.

It is remarked that no straight steel fiber results are included and compared with the attained results in this present investigation. This due to, firstly, the intercept mechanism and inhibition of crack growth reducing the likelihood of further crack propagation are different. Besides, this is reasonably reported in literature, which will negatively work with the novelty of this investigation.

Table 1. Physical characterization of the materials used in the composition of the concretes.

Physical properties	Cement	Silica fume	Fine aggregate	Coarse aggregate	Marble/granite (MGR)	Rubber residues	SP
Density (g/cm³)	3.08	2.21	2.65	3.01	2.58	1.16	1.08
Unit weight (g/cm³)	1.03	-	1.50	1.51	-	0.39	-
Max Diameter (mm)	-	-	1.20	9.50	0.10	2.40	-
Fineness modulus	-	-	1.76	5.47	10.28	2.82	-
Water absorption (%)	-	-	0.20	1.40	-	-	-

 doi:10.20944/preprints202405.1143.v1

Table 2. Chemical compositions of cement, silica fume, MG, and rubber. All values are varying up to 10% from those absolute values.

	Cement	Silica fume	Marble/granite (MG)	Rubber residue
Chemical composition (%)				
CaO	63.33	0.36	14.3	-
SiO_2	19.19	95.61	48.2	-
Al_2O_3	5.15	0.17	12.0	-
Fe_2O_3	2.8	0.08	5.13	-
MgO	0.92	0.55	2.82	-
Na_2O	-	0.19	2.03	-
K_2O	-	1.29	3.77	-
TiO_2	-	-	1.17	-
Lost on ignition	8.13	1.75	10.58	-
Insoluble residue	0.48	-	-	-
Chemical element (%)				
C	-	-	-	91.5
Zn	-	-	-	3.5
O	-	-	-	3.3
S	-	-	-	1.2
Na	-	-	-	0.2
H	-	-	-	0.2
Ca	-	-	-	0.1

2.2. Production of Concrete

After the wheel design six distinctive SCC mixtures are proposed. The purpose is to demonstrate the effects of the MGR content associated with HESF and the rubber in both the fresh and hardened states of the SCC samples examined. The selection of mixes is based on dosage studies for SCC developed by [11,12,49-50]. The content of silica fume used in the mixtures is 10% concerning the cement mass, the water/cement ratio was 0.58, and the mortar content is close to 65%. Two distinct fiber consumptions are adopted, that is, 10 (±1) kg/m^3 and 20 (±1) kg/m^3. The dosages adopted for fibers are based on previously reported studies [24, 51-52].

Table 3 shows the mixtures of the studied concretes. In order to guarantee reproducibility and to determine the compressive strength, for each one of the proposed mixtures, at least 6 specimens are molded and tested at 7 and 28 days of age. Thus, the number of the used specimens to conduct the compression, tensile and modulus of elastic measurements are 10, 4 and 4, respectively. This totalizes 60 + 24 + 24 = 108 specimens considering all proposed mixtures.

To determine Young's moduli and damping of distinct proposed samples, 06 specimens are elaborated. A concrete mixer at environmental temperature of about 20 (±5) ^{o}C is used in order to the concrete mixing be proceeded.

During the molding stage, the concretes are placed into metallic molds. After 24 hours of curing the specimens are withdrawn from molds and subjected to the wet curing process at controlled environmental temperature (~23 ± 2) ^{o}C, and the relative humidity kept at 95%. The specimens are kept under curing condition until the period to the mechanical tests be carried out (i.e. at 28 days after molding). It is known that a disadvantage of SCC is the lack of cohesion of the cement paste and, consequently, the coarse aggregates are heterogeneously segregated. To avoid this occurrence, the MGR content is used. In this research, marble is used to increase cohesion and to decrease the segregation [30]. It is remarked that superplasticized is maintained at 2 % for all examined samples. However, the water-to-cement ratios of the SCC/20SF/30MGR and SCC/20SF/30MGR/5R samples are slightly lower.

 doi:10.20944/preprints202405.1143.v1

Table 3. Concrete mixture proportions, results of the fresh and hard states tests of the mixtures. All values are ranging up to 10% from those absolute values.

	SCC/10SF	SCC/10SF/30MGR	SCC/10SF/30MGR/2.5R	SCC/20SF	SCC/20SF/30MGR	SCC/20SF/30MGR/5R
Cement (kg/m³)	366	366	366	365	350	345
Silica fume (kg/m³)	37	37	37	37	35	35
MG (kg/m³)	0	110	110	0	105	104
Rubber (kg/m³)	0	0	9	0	0	17
Sand (kg/m³)	1036	922	904	1033	991	976
Coarse aggregate (kg/m³)	761	761	761	759	728	718
Steel fiber (kg/m³)	10	10	10	20	20	20
Water (kg/m³)	212	212	212	212	203	200
Superplasticizer (%)	2	2	2	2	2	2

2.3. Fresh State and Hardened States Measurements

The properties of the SCC specimens in the fresh state are evaluated according to the Brazilian standard ABNT NBR 15823-1:2017, which has international equivalence standard. Slump-flow, flow time and visual stability index tests (Abrams cone method) are carried out, as described in ABNT NBR 15823-2:2017. Both J-ring and V-funnel methods are also described in ABNT NBR 15823-3:2017. These procedures are carried out with the purpose to evaluate the workability of the SCC and the ability to pass through obstacles [24].

Compressive strength are carried out utilizing cylindrical specimens 100 x 200 (± 1) mm acording to ABNT NBR 5739:2018. The tensile strength is determined by using also cylindrical specimnes utilizing a dimetrical compression method (ABNT NBR 7222:2011) and modulus of elasticity by the compression (ABNT NBR 8522:2017). For these purposes, a universal testing machine, with a load capacity of 600 (±5) kN. Cylindrical specimens at 28 days are used to carry out the water absorption tests by immersion, voids index and specific mass. In the same way, the dynamic moduli of elasticity are determined, as well as the damping rate by the Impulse Excitation Technique (ASTM C215: 2014 and ASTM E1876:2015). This constitutes a non-destructive test in which the moduli of elasticity are measured from the natural frequencies of the vibration of the sample with a regular geometry (cylindrical samples 100 x 200 mm, ± 1 mm). The acoustic tests are carried out according to the arrangement shown in Figure 3 (a). The specimens are supported on two steel cables, with tension and adjustable positions on the rigid support (manufactured by ATCP - Sonelastic®, ATCP Physical Engineering 735A Leda Vassimon, 14026-567, Ribeirão Preto, Brazil; www.atcp-ndt.com) support for bars and cylinders. This support is accordance with the requirements of ASTM E1876:2015.

In this study, the steel cables are positioned at a distance of 0.224 x L from their ends, where L is the length of the specimen to simulate the specific condition of free-free contour. The specially developed hammer, with rubber handle and a steel ball at the end, is used to apply manual external excitation. The rubber cable has appropriate dynamic characteristics, such as very low natural frequencies and high damping so as not to interfere with test measurements. The steel sphere with a diameter of 12.7 (±0.2) mm proved to be very effective in providing sufficient impact energy to excite the frequencies in the range of interest. A microphone (directional acoustic sensor CA-DP with specific technical characteristics designed by enterprise ATCP Physical Engineering) to capture the acoustic response transmitted by the surface of the specimen is used. The dedicated software made it possible to adjust acquisition parameters, such as sampling rate, filtering and windowing, so that natural frequencies are adequately identified and extracted with precision.

From the acoustic response caused by the short-term mechanical impact on the specimen and, based on its mass, geometry and dimensions, the dynamic modulus of elasticity is calculated, as shown in Figure 3(a). The damping is calculated using the logarithmic decrement method (Figure 3b), which consists of the ratio between two successive amplitudes of the signal. For this purpose, a viscoelastic damping model is considered [53]. The response time of an oscillatory system with a degree of freedom, with viscous damping when excited by an impulse is described in Equation (1):

Preprints.org (www.preprints.org) | NOT PEER-REVIEWED | Posted: 17 May 2024 doi:10.20944/preprints202405.1143.v1

$$z(t) = z\,(e^{-\zeta\omega_0 t})\sin(\omega_d t) \qquad (1)$$

where z (μm), ω_0 and ω_d (expressed in Hz) represent the natural frequency of vibration and damped natural frequency, as prescribed in Equation (2).

$$\omega_d = \omega_0\sqrt{1-\zeta^2} \qquad (2)$$

Considering the responses at moments $t = t_n$ (enesimal time, seconds) represented by A (μm) and $t = t_n + 2\pi\ r/\omega_d$, with r being period, expressed by A_n (μm), Equation (3) is obtained (Figure 3b):

$$\frac{A_n}{A} = \exp\left(-\zeta\frac{\omega_0}{\omega_d}2\pi n\right) = \exp\left[-\frac{\zeta}{\sqrt{1-\zeta^2}}2\pi n\right] \qquad (3)$$

Therefore, the logarithmic decrement (δ) is obtained as followed in Equation (4):

$$\delta = \frac{1}{n}\ln\left(\frac{A}{A_n}\right) = \frac{2\pi\zeta}{\sqrt{1-\zeta^2}} \qquad (4)$$

and the damping factor (ζ) is obtained by Equation (5):

$$\zeta = \frac{1}{\sqrt{1+(2\pi/\delta)^2}} \qquad (5)$$

When the damping is small (ζ < 0.1), the damping frequency is almost equal to the natural frequency, that is, $\omega_d \cong \omega_0$, $_0$, and then Equation (3) is reworked, as shown Equation (6):

$$\frac{A_n}{A} \cong \exp(-\zeta 2\pi n) \qquad (6)$$

or, as expressed by Equation (7) when ζ < 0.1, as followed:

$$\zeta = \frac{1}{2\pi\,n}\ln\left(\frac{A}{A_n}\right) = \frac{\delta}{2\pi} \qquad (7)$$

The dynamic deformation modulus is approximately equal to the initial tangent modulus determined in the static test [54-55]. This relationship is not easily determined based on physical behavior, as the heterogeneities of the two moduli are differently affected, as previously reported [55].

Some empirical expressions relating the static (Es) and dynamic (Ed) moduli reported (both expressed in MPa) at BS 8110-2:1985 [56]. Considering the concrete with cement content of less than 500 kg/m³ or for concrete with normal density aggregates, the static modulus, in MPa, is expressed by Equation (8).

$$E_S = 1.25 \times E_d - 19 \qquad (8)$$

Lyndon and Baladran [57] have reported Equation (9) to describe the E_S, as follow:

$$E_S = 0.83 \times E_d \qquad (9)$$

On the other hand, Popovics [58] has reported Equation (10), as followed:

$$E_S = \kappa \times E_d^{1.4} \times \rho^{-1} \qquad (10)$$

where ρ is the specific mass (kg/m³) of the concrete and κ is a constant that depends on the units of measurement.

 doi:10.20944/preprints202405.1143.v1

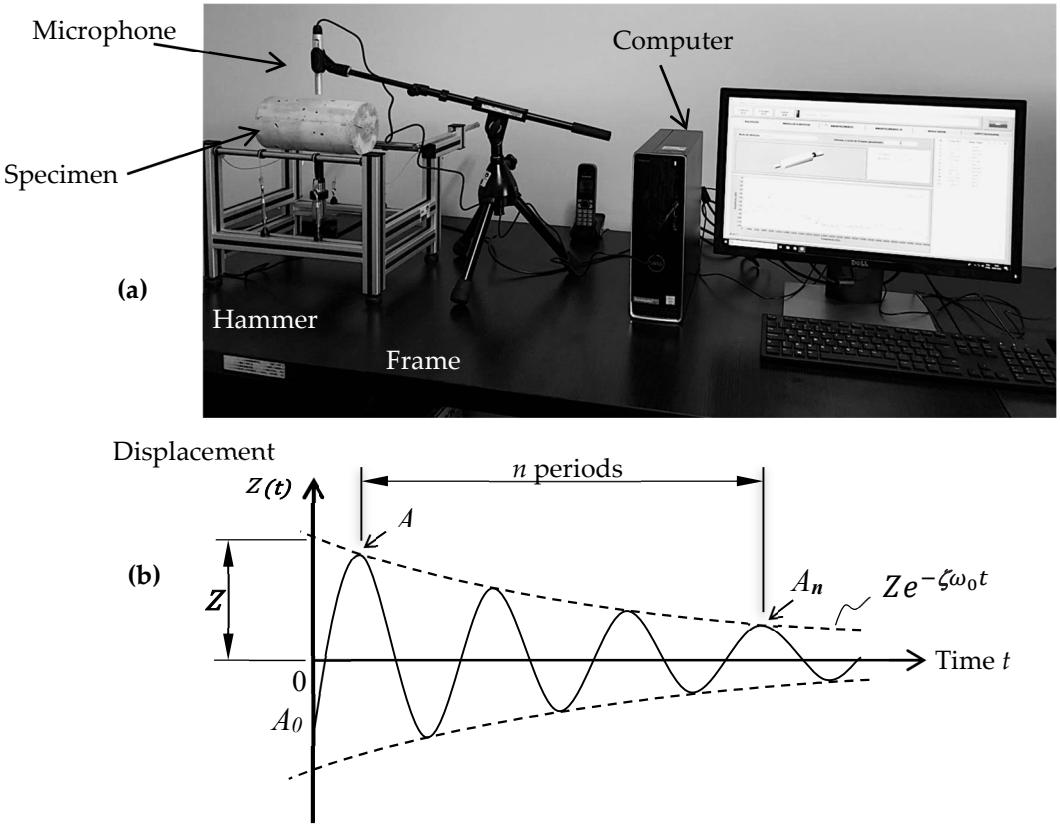

Figure 3. (a) Photograph representing the dynamic testing by impulse stimulus (damping and dynamic elastic modulus); and **(b)** Response to the impulse of a damped system with a degree of freedom $0 < \zeta < 1$ at time $t = 0$, adapted from [60].

2.4. Microstructural Characterizations

In order to characterize the examined samples which were prepared by using distinctive mixtures, a scanning electron microscope, SEM (TESCAN® model VEGA3, Brno, Czech Republic) coupled with an energy-dispersive x-ray spectroscopy (EDS) is utilized. All samples are withdrawn from the representation regions, which are intended to be characterized. Also, at least, duplicate is considered to provide reproducibility of the attained analyses. It is remarked that a gold sputtering (model MEV LEO 430i, Zeiss, USA) is used to prepare the surface sample of the each specific condition. Majority observations are obtained using electron beam energy of 20 kV, beam current of 500 pA and a working distance: ~19 mm.

3. Results and Discussion

3.1. Fresh State Properties

The experimental results of the fresh state of the examined SCC samples are shown in Table 4. With respect to the spreading test, all the concretes produced in this study are in accordance with the specifications of the Brazilian standards of ABNT NBR 15823-1:2017. A minimum limit attained value of 550 (±2) mm and maximum 850 (±2) mm for slump flow are required. It is observed that the mix containing rubber shows a spreading value decreased for both the group with 10 kg/m^3 and 20 kg/m^3 of steel fibers contents. For the SCC/20SF/30MGR/5R sample, a lower spreading value than other examined samples is attained. This seems to be associated with the higher fiber content (20 kg/m^3) and greater amount of the rubber waste. Considering the visual stability index, neither segregation nor exudation is observed. These results of the fresh state are similar to those previously published [14, 16, 35, 54].

 doi:10.20944/preprints202405.1143.v1

Table 4. Properties in the fresh state of the SCC. Error values are up to 10%.

	SCC/10SF	SCC/10SF/30MGR	SCC/10SF/30MGR/2.5R	SCC/20SF	SCC/20SF/30MGR	SCC/20SF/30MGR/5R
Slump flow (mm)	730	837	725	735	725	595
T_{500} (s)	1.10	1.86	1.40	1.00	2.00	3.00
J-ring (mm)	20.00	25.00	5.50	17.50	15.75	6.25
V Funnel (s)	3.10	3.18	4.20	8.00	4.10	8.00

Based on the experimental results of the V-funnel, fluidity and viscosity, the samples containing rubber content, *i.e.* designated as the SCC/10SF/30MGR/2.5R and SCC/20SF/30MGR/5R samples, higher flow times results are observed than the groups with 10 kg/m^3 and 20 kg/m^3 steel fiber contents. All the examined SCC samples are classified as VF 1. This means that the reached value is less than or equal to 8 s. Based on the J-ring results, all mixtures have shown values equal to or less than 25 (±0.5) mm. This induces that a good ability to pass through obstacles is attained and a classification PJ 1 is indicated.

The parameter T500 is recognized as a flow test providing the time required to concrete flows and reach a spreading inside a 500 circle. By using this result, it possible to classify the mix as VS1 excepting the SCC/20SF/30MGR/5R sample, which is classified as VS2 due to the higher rubber and steel fiber contents (20 kg/m^3). Bušic *et al.* [36] have also observed that the passing ability is reduced with the rubber residues addition.

It is worth noted that the concatenated use of the HESF + rubber + marble and granite residues in SCC has not previously been reported. Since its properties in the fresh state are satisfactory, the properties in the hardened state are determined.

3.2. Hardened State Properties

Table 5 shows the experimental results obtained in the tests in the hardened state of the SCC. Considering the results of the compressive strengths, the obtained values reveal that values higher than 34 (±2) MPa at 7 days are attained. Since HES cement is used, it is recognized that a more rapid hydration is provided. Besides, higher cohesion than conventional cement (ordinary Portland) is also reached [61-62].

Table 5. Experimental results of hardened states of the examined samples at 7 and 28 days.

Sample	**Compressive strength, CS (MPa)**		**Tensile strength, TS (MPa)**	
	7 days	**28 days**	**7 days**	**28 days**
SCC/10SF	58.1 (±1)	73.3 (±1.4)	5.7 (±0.2)	6.4 (±0.2)
SCC/10SF/30MGR	57.3 (±1)	73.3 (±3.2)	5.8 (±0.3)	6.8 (±0.5)
SCC/10SF/30MGR/2.5R	49.9 (±1.5)	62.7 (±3.1)	5.4 (±0.6)	5.6 (±0.4)
SCC/20SF	50.0 (±2)	71.0 (±2.0)	6.0 (±0.2)	6.1 (±0.1)
SCC/20SF/30MGR	55 (±2)	72.7 (±2.6)	5.7 (±0.3)	7.2 (±0.1)
SCC/20SF/30MGR/5R	34.9 (±2.7)	45.5 (±1.9)	4.1 (±0.2)	5.3 (±0.7)

It is recognized that all studied concrete compositions are commonly classified as structural concrete according to ABNT NBR 8953:2015. Excepting the sample with 5% rubber (SCC/20SF/30MGR/5R), all other samples indicate the group II class, which has compressive strength ≥ 55 MPa being considered high strength concrete, at 28 days. In a previous investigation developed by Aïtcin [63], it is classified as high-performance concrete, *i.e.* class I (between 50 and 75 MPa).

Regarding the addition of the MGR content into the mixture, a low increase in the compressive strength of the SCC/20SF/30MGR mixture is observed when the SCC/20SF sample is compared. The MGR consumption of 105 kg/m^3 for the SCC/20SF/30MGR mixture evidences that no substantial modification is verified, even with the decrease in cement consumption (350 kg/m^3). This seems to be compensated by the MGR content, resulting in a slight increase (of about of 2.5%) in the compressive

 doi:10.20944/preprints202405.1143.v1

strength when the SCC/20SF sample is compared. This correlates with the reduction of the pores of the cement paste, since the MGR portion fills these voids, providing more cohesion of the paste and increasing the packaging of the concrete.

However, the values obtained for the SCC/10SF and SCC/10SF/30MGR samples are very close. The MGR consumption of 105 kg/m^3 for the SCC/10SF/30MGR sample has not affected the compressive strength when the SCC/10SF sample is compared. This has occurred probably due to the sand portion is replaced with the MGR content. Interesting that a cement consumption of 366 kg/m^3 is maintained.

The compressive strengths of the group with HESF consumption of 10 kg/m^3 (SCC/10SF, SCC/10SF/30MGR, SCC/10SF/30MGR/2.5R) have shown higher values than the group with HESF consumption of 20 kg/m^3 (SCC/20SF, SCC/20SF/30MGR, SCC/20SF/30MGR/5R). This indicated that the increase of the fiber rate has no affect this property, according to previous studies [22-24].

For the sample of the group with HESF consumption of 10 kg/m^3, the cement consumption is kept constant (366 kg/m^3), and the sand portion is replaced with both the rubber and MGR residues contents. This has provided a compressive strength higher than the group with 20 kg/m^3 of HESF and cement consumption of 365 kg/m^3 (the SCC/20SF sample), 350 kg/m^3 (the SCC/20SF/30MGR sample) and 345 kg/m^3 (the SCC/20SF/30MGR/5R sample).

It is also found that the compressive strength is strongly affected in mixtures containing rubber residue, *i.e.* the SCC/10SF/30MGR/2.5R and SCC/20SF/30MGR/5R samples. The lowest compressive strength is that of the SCC/20SF/30MGR/5R sample. It corresponds to a decrease of about 36% when the SCC/20SF sample is compared. The SCC/10SF/30MGR/2.5R mixture has shown a 14.5% reduction in the compressive strength when compared with the SCC/10SF sample. The decrease in compressive strength with the increase of rubber content is also previously reported [16, 37, 39, 64-66]. This occurrence is attributed to two main reasons: (a) firstly, the cracks are rapidly initiated at neighboring the rubber particles and concrete paste, and (b) the rubber particles are weakly adhered to the paste, behaving like voids in the concrete matrix [16, 64].

Regarding the tensile strength, this property is less affected than the compressive strength for all mixtures examined. Considering the rubber compositions, a decrease of about 13% is verified for the SCC/10SF/30MGR/2.5R sample when the SCC/10SF is compared. Similarly when the SCC/20SF/30MGR/5R and the SCC/20SF samples are also compared. In previous studies this behavior is also reported [16, 23, 64-65]. From this point, it is important to remark the decision to rubber content be adopted in the proposed mixture examined in the present investigation. Although it is recognized that rubber potentially decreases compressive behavior, certain improvements in tensile strength can be attained [61-62; 64-66]. Based on this previous perspective the rubber contents were considered to prepare other mixtures containing rubber contents.

Table 6 shows, at 28 days of age, the static moduli of elasticity of the SCC/20SF and SCC/20SF/30MGR samples are very similar. Similarly, this also occurs when the SCC/10SF and the SCC/10SF/30MGR samples are compared. Comparing the mixtures without residues, the SCC/20SF and SCC/10SF samples have revealed a decrease or difference of about of 2.5%. When the rubber compositions are considered, the decreases are ~22% for the SCC/20SF/30MGR/5R when compared to the SCC/20SF sample; and of about 6% for the SCC/10SF/30MGR/2.5R sample when the SCC/10SF sample is considered.

Table 6. Experimental results of the damping ratio and the moduli of elasticity determined by static and dynamic using IET of the examined SCC samples at 28 days.

Sample	Static Modulus (GPa)	Dynamics flexural modulus (GPa)	Dynamics Longitudinal modulus (GPa)	Damping ratio ζ (%)
SCC/10SF	39.8 (±1.2)	44.4 (±1.6)	43.7 (±1.3)	0.34 (±0.01)
SCC/10SF/30MGR	40.2 (±1.7)	45.6 (±0.2)	44.9 (±0.6)	0.34 (±0.02)
SCC/10SF/30MGR/2.5R	37.4 (±1.6)	42.5 (±0.7)	41.7 (±0.6)	0.35 (±0.01)
SCC/20SF	40.7 (±1.9)	45.5 (±0.5)	44.8 (±0.5)	0.37 (±0.01)

 doi:10.20944/preprints202405.1143.v1

SCC/20SF/30MGR	40.1 (±0.6)	45.9 (±0.5)	45.4 (±0.3)	0.35 (±0.01)
SCC/20SF/30MGR/5R	31.4 (±1.2)	35.1 (±0.6)	35.0 (±0.5)	0.38 (±0.01)

Aslani and Kelin [23] have found that with the increase of the steel fiber content in a SCC, an increase of the elasticity modulus is attained. On the other hand, Hilal [16] has also found that the static elastic modulus has decreased with the increase of the rubber content, similar to that observed for both the tensile and compressive strengths. Based on the fact that the dynamic longitudinal modulus is lower than the flexional, the longitudinal dynamic modulus is considered. The non-destructive method (IET) presents values of the longitudinal dynamic elasticity moduli higher than the static moduli, at 28 days of age, as shown in Table 6 and Figure 4 (a).

This fact is associated with the IET method, which consists in determining the natural vibration frequencies of the concrete specimen, in the free-free condition, through excitation by a slight mechanical impact. This mechanical excitation applied to the specimen produces very low stress levels during the determination of these parameters; therefore, the formation of microcracking and creep effect is not provided. For these reasons, it can be considered that the dynamic modulus is associated only with elastic phenomena of the material and is closer to the initial tangent modulus. This corresponds to the elastic behavior of the concrete obtained at the beginning of the stress strain curve [54-55]. The values of dynamic moduli are usually higher than static moduli due to the period of time characteristic of the vibration used in dynamic methods is regularly less than 1 millisecond (ms). With this, the occurrence of annelastic mechanisms with a relaxation time higher than 1 ms is prevented [67].

The IET method has some advantages when compared to the static method. The non-destructive test has reproducibility in a short period using the same sample. Therefore, a smaller amount of samples is required and less susceptibility to experimental errors due to the number of variables is provided [68].

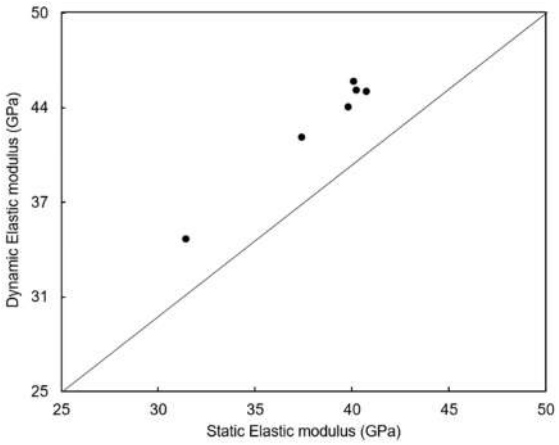

(**a**)

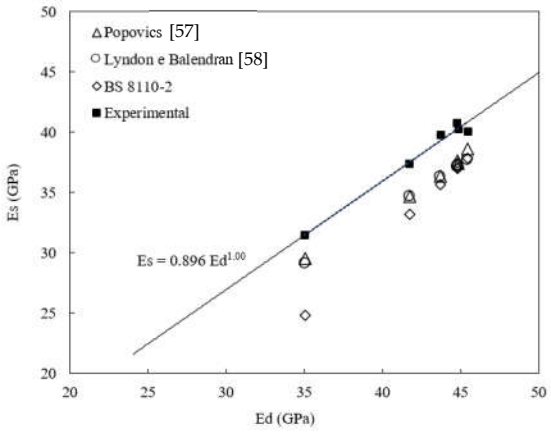

(**b**)

 doi:10.20944/preprints202405.1143.v1

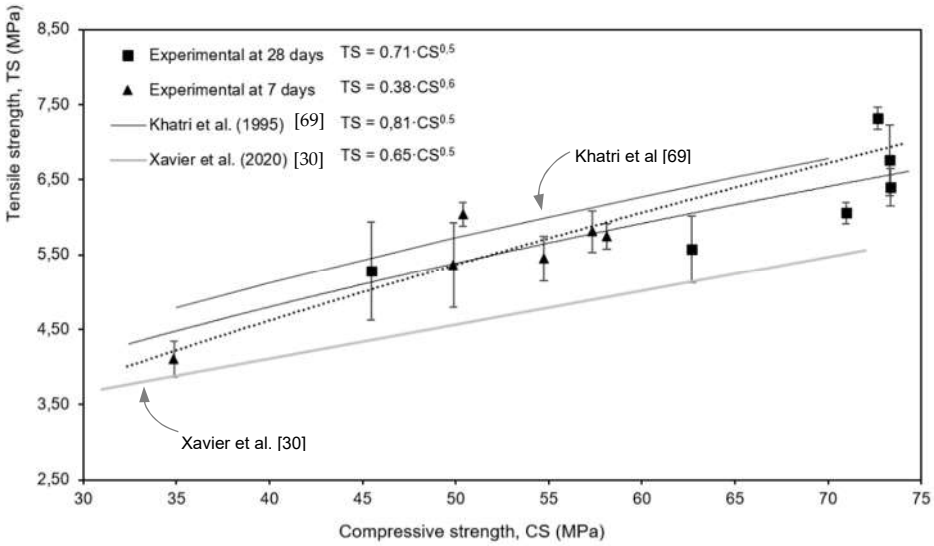

(**c**)

Figure 4. (a) Relation between dynamic modulus and static modulus of the SCC samples, **(b)** considering some empirical concerning to static modulus and dynamic modulus and **(c)** tensile-to-compressive strength ratios.

Figure 4 (b) shows the results of some empirical data realted with the attained static (Ec) and dynamic (Ed) and compared with previously reported results of Popovics [58], Lyndon and Baladran [57], and prescribed into BS 8110-2:1985 [56]. It is observed that the experimental values of dynamic (Ed) and static moduli (Es) of the SCC compositions examned, the follow correlation is attained, i.e., $Es = 0.896 \times Ed^{1.0}$ associated with $R^2 = 0.99$. It is observed that the experimental values are overestimating those previously reported [56-58]. The variability of the results is justified by the multiphase nature of the concrete, which influences the mechanims that it deforms.

Figure 4 (c) shows the correlation considering an exponential dependence of the tensile property with the compressive strength at 7 days (expressed by $TS = 0.38 \times CS^{0.6}$) and at 28 days (expressed by $TS = 0.71 \times CS^{0.5}$). Khatri *et al*. [69] and Xavier *et al.* [30] have reported similar correlations when silica fume/furnace slag/fly ash and MGR contents are used, respectively. The equations proposed in this present study of both the experimental results at 7 and 28 days, are located between the upper and lower limits proposed.

The experimental results at 28 days of compressive strength as a function of porosity is shown in Figure 5. The Ryshkewitch's equations are described, $CS = 58\exp(-0.082\,P)$, and the experimental results at 28 days, $CS = 211.21\exp(-0.111\,P)$. Similar trends are observed.

Preprints.org (www.preprints.org) | NOT PEER-REVIEWED | Posted: 17 May 2024 doi:10.20944/preprints202405.1143.v1

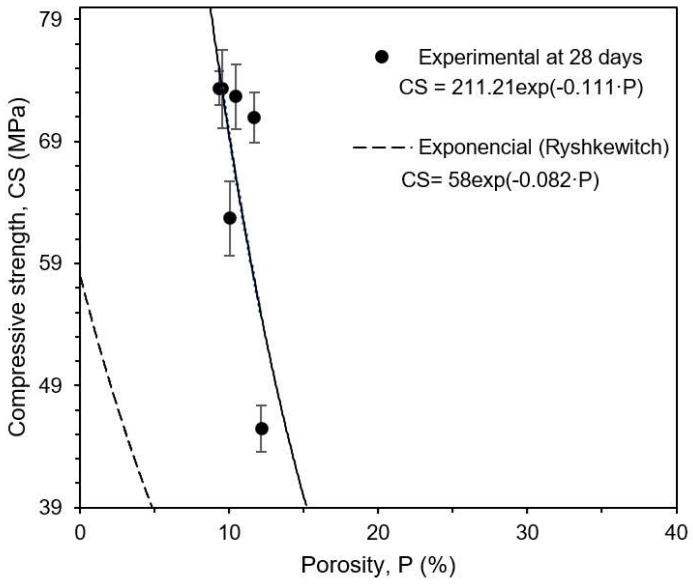

Figure 5. Ryshkewitch's equation describing the compressive strength (CS) as a function of porosity (P) considering 28 days of curing.

Table 6 shows the values obtained in the experimental tests of the damping factor of the SCC samples examined. The damping factor of the studied SCC is higher than steel and cast iron. The damping rate of the steel is reported between 0.001 and 0.002 [70] and the corresponding value to the cast iron is of about 0.0023 [71]. Regarding to the SCC/20SF sample (with a consumption of HESF being of 20 kg/m^3) and the SCC/10SF (with HESF consumption of 10 kg/m^3), it is observed that with the increase of HESF consumption, the damping factor is of about 9% increased, as shown in Table 6. However, there is a decrease in this property for the SCC/20SF/30MGR and SCC/10SF/30MGR samples when the SCC/20SF and SCC/10SF samples are compared, *i.e.* of about 6% and 2%, respectively.

With regard to the SCC/20SF/30MGR/5R and the SCC/10SF/30MGR/2.5R samples, a slight increase of 1.34% is observed when the SCC/20SF/30MGR/5R and the SCC/20SF samples are compared. When the SCC/10SF/30MGR/2.5R sample is compared with the SCC/10SF samples, the observed difference is of about 2.6%.

Considering those samples containing both MGR content and rubber residue portions, *i.e.* 2.5 and 5%, the two highest reached values (0.35% and 0.38%, respectively) of damping factors are associated with these mentioned samples, *i.e.* designated as the SCC/10SF/30MGR/2.5R and the SCC/20SF/30MGR/5R samples. This suggests that a better energy dissipation capacity is provided when the modified concrete is subjected under a dynamic load, as previously reported [12, 39, 72].

The rubber portion, when incorporated into the concrete, certain voids into the paste are prevalent, and consequently the resulting porosity is increased. The experimental results of the specific mass, voids index and water absorption by immersion, measured accordingly to ABNT NBR 9778:2009, are shown in Table 7. The observation of the attained values shown in Table 7 clarifies that both the HESF and rubber contents provides the highest values of both the water absorption and voids (porosity).

Table 7. Experimental results of density, water absorption and void index tests.

	SCC/10SF	SCC/10SF/30MGR	SCC/10SF/30MGR/2.5R	SCC/20SF	SCC/20SF/30MGR	SCC/20SF/30MGR/5R
Water absorption (%)	4.02 (±0.08)	4.08 (±0.06)	4.40 (±0.01)	5.04 (±0.57)	4.53 (±0.03)	5.80 (±0.12)
Voids index (%)	9.33 (±0.17)	9.55 (±0.09)	10.04 (±0.08)	11.68 (±1.27)	10.45 (±0.07)	12.16 (±0.21)

 doi:10.20944/preprints202405.1143.v1

Specific mass (kg/m³)	2320 (±3.48)	2339 (±17.05)	2280 (±15.66)	2319 (±12.58)	2306 (±3.48)	2097 (±12.04)

Figure 6(a) shows the influence of porosity in relation to the damping rate. Thakare *et al.* [72] have also found that the air entrapped in fresh mortars is increased with rubber fibers incorporation. Based on these previous assertions and attained experimental observations, it is induced that a SCC containing rubber residue has the porosity increases, associated with decreasing in the compressive strength, the tensile strength and the dynamic modulus. On the other hand, it is clarified that the damping has appreciably increased.

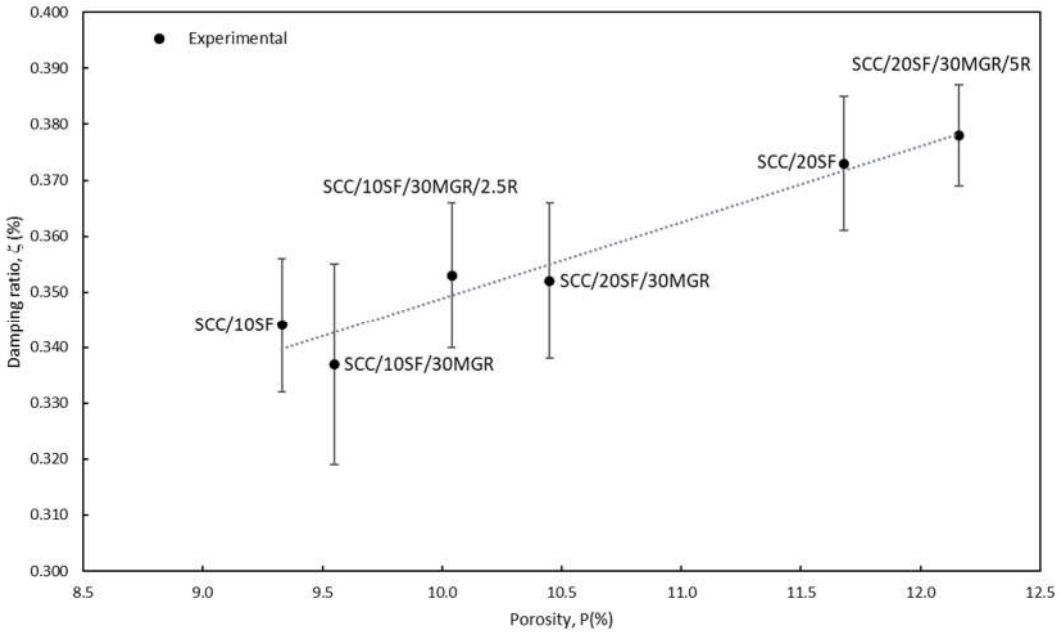

(**a**)

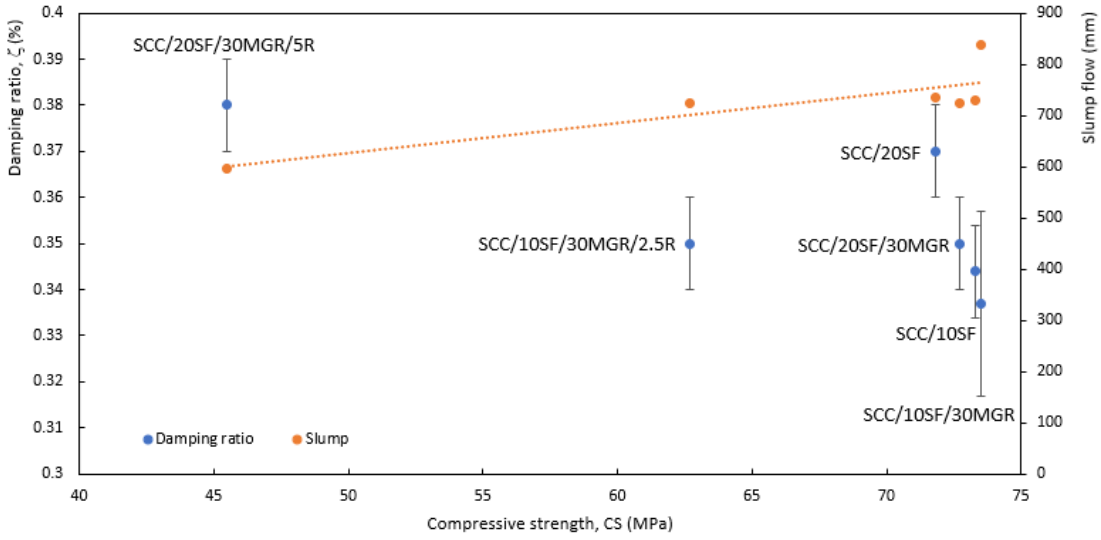

(**b**)

Figure 6. (a) Experimental damping ratio as a function of the porosity level, and **(b)** reveals damping ratio and slump flow variations with compressive strengths for all examined concrete samples.

Li *et al.* [12] have concluded that the SCC damping rate increases linearly with the rubber content. This suggests that a better energy dissipation capacity is attained when subjected to dynamic

 doi:10.20944/preprints202405.1143.v1

load. Najim and Hall [39] have also found that the damping coefficient increases with the increase of rubber content in the mixture.

Based on aforementioned results, it is considered interesting to analyze the concatenated effects of the MGR and HESF contents up on two main important properties of a SCC, *i.e.* slump (fresh property) and compressive strength (hardened property). Besides, considering the fact that, at under certain determined condition, the damping should also be considered, both slump flow and damping are evaluated. The experimental variations of slump flow and damping ratio as a function of the compressive strength are demonstrated in Figure 6(b). This due to the slump flow and damping seems to be competitive properties mainly when the MGR and HESF contents are increased.

Considering that a design of mixture requires compressive strength in a magnitude between 70 and 75 MPa, the HESF content has no substantial effect on the slump flow results. However, the MGR content clarifies that slump flow can slightly be improved mainly the HESF portion is increased. This is observed when the same magnitude of compressive strength (between 70 and 75 MPa) is considered. Also considering this same range of compressive behavior, the damping results reveal that the 30 MGR content has a deleterious effect. Interesting, the HESF content demonstrates a positive effect on the damping.

For instance, the SCC/20SF has a damping considerably higher (~9%) than SCC/10SF sample. Similarly, when analyzing the SCC/10SF/30MGR and SCC/20SF/30MGR samples, the damping results reveal that, although, 30MG content is present in both mixtures, the sample with higher steel fiber content (*i.e.* SCC/20SF/30MGR) has evidenced higher damping (~7%) than other one. On the other hand, when the SCC/20SF is compared with the SCC/20SF/30MGR, and the SCC/10SF with the SCC/10SF/30MGR, the effect of the MGR content is indicated. It is revealed a deleterious effect of the MGR content up on the damping results, *i.e.* it decreases of about 6%. Additionally, when lower range of the compressive strength is acceptable in a certain design mixture, for instance between 40 and 50 MPa, it is induced that the slump flow and damping ratio are competitive properties. The highest damping ratio is that of the SCC/20SF/30MGR/5R samples, while their corresponding slump flow result is the lowest attained result. The increase of the damping is intimately associated with 20SF content and the considerable decrease (~20 %) of their slump flow is attributed to rubber content, as also shown in Fig 6(b). It is previously reported that rubber content, depending of some limited characteristics and condition, in a general way, the rubber content provides a deleterious effect on mechanical behavior [61-65; 72-77]. Also, it is reported that the steel fiber content (up to certain limits) improves the damping behavior [78], as also observed in this study.

When the SCC/20SF/30MGR/5R and the SCC/10SF/30MGR/2.5R samples are compared, it is remarked that the SF content increases damping results while rubber content decreases the slump flow. Associated to this a considerable and substantial decrease of the compressive strength (~38%) is observed. This is also associated with double rubber content in the SCC/20SF/30MGR/5R sample, as also depicted in Figure 6(b). Summarizing, it is worth noting that the rubber addition induces to certain worsening in the compressive strength of concrete.

In the next section, the micrographs of the reinforced concretes using SEM technique demonstrate that the concrete with rubber content, various microcracks are constituted. Also, it is shown that HESF has an interface with cement paste without “voids”, as forwardly described and discussed.

3.3. SEM Micrographs of the Examined SCC

Figure 7 shows the microstructure of the SCC samples examined in different magnifications. Comparing Figures 7 (b) and 8 (d) with the mixtures depicted in Figures 7(a) and 7 (c), it is noted that the compositions with marble and granite residues (SCC/10SF/30MGR and SCC/20SF/30MGR) provide their corresponding cement pastes denser and more consolidated with aggregates and fibers than other ones. The hexagonal plates of calcium hydroxide (CH) and calcium silicate hydrate (C-S-H) particles are also characterized.

Commonly, a higher amount of calcium and silica induces to the substantial formation of C-S-H gel in a mixture. In addition, these associated residues increase the consolidation of the

 doi:10.20944/preprints202405.1143.v1

microstructure. These constituted particles are finer than the aggregates. Consequently, the voids are filled and improve the packaging, providing a compact structure, and both the quantity and the sizes of the pores are decreased. This corroborates with a lower void index and water absorption, confirming the experimental values obtained.

It is also found that no interfacial transition zone (ITZ) is clearly characterized. The interaction at interface between steel fiber and cement paste seems to provide a corrosion layer formation. This migrates to cement paste forming a corrosion-filled paste region, without ITZ constitution, as previously reported [30; 79-80]. All these assertions working in corroborative mechanism seem to be responsible for the observed gain of the mechanical behavior, as demonstrated in Tables 5 and 6. This behavior is also previously observed [11; 30]. Typical SEM micrographs of the SCC/10SF/30MGR/2.5R (with 2.5% rubber residues) and the SCC/20SF/30MGR/5R samples (with 5% rubber residues) are shown in Figure 8 (a) and 8(b). An open structure with crack propagation is depicted. Also, a clear characterized transition zone, with an increase in the volume of large voids is also shown. This has occurred due to the incorporation of the rubber residue and entrapped air. It is remembered that the highest void index and water absorption is that of examined sample, as demonstrated in Table 7.

Associated with these values, lower compressive and tensile strengths and modulus of elasticity are observed. Additionally, the highest damping factor is also observed, as shown in Tables 5 and 6. The same characteristics are verified in relation to the microstructure corresponding with the rubberized concretes, as previously reported [73-77].

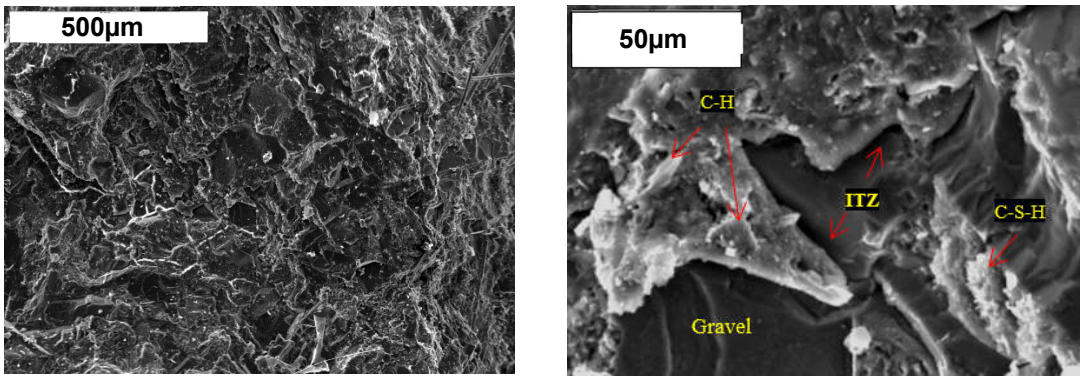

(a) SCC/10SF

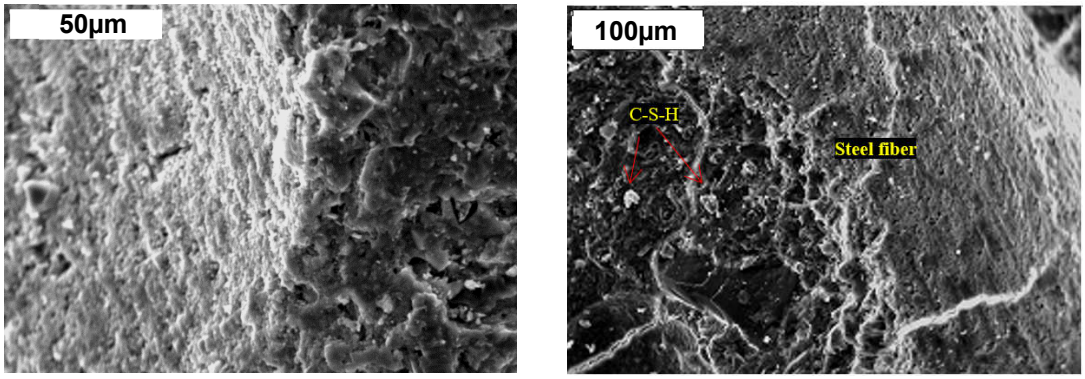

(b) SCC/10SF/30MGR

 doi:10.20944/preprints202405.1143.v1

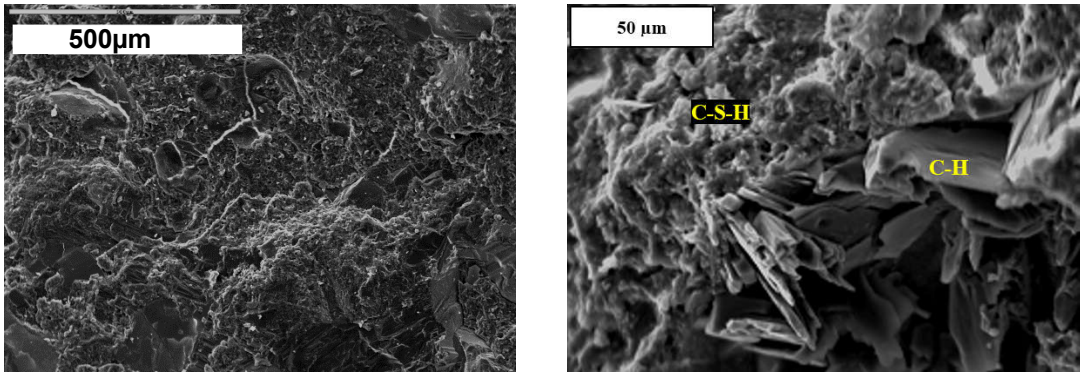

(c) SCC/20SF

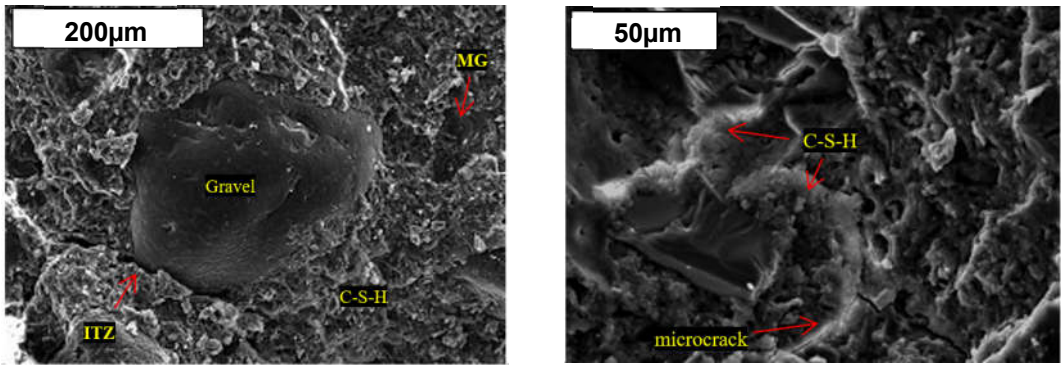

(d) SCC/20SF/30MGR

Figure 7. SEM (SE technique) images of concrete mixes with distinct steel fiber contents and MGR: **(a)** the SCC/10SF, **(b)** the SCC/10SF/30MGR, (**c**) the SCC/20SF and **(d)** the SCC/20SF/30MGR samples.

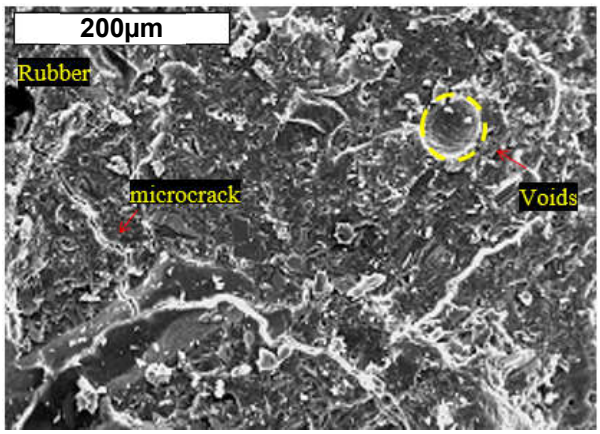

(a) SCC/10SF/30MGR/2.5R

 doi:10.20944/preprints202405.1143.v1

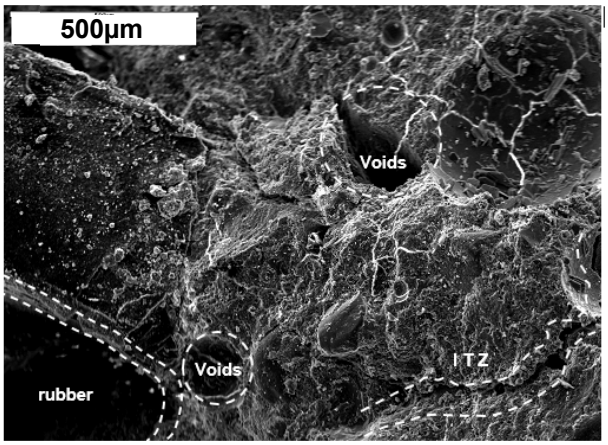

(b) SCC/20SF/30MGR/5R

Figure 8. SEM(SE technique) images of concrete mixes with distinct steel fiber contents, MGR and rubber: **(a)** the SCC/10SF/30MGR/2.5R sample, and **(b)** the SCC/20SF/30MGR/5R sample.

4. Conclusions

Based on the attained experimental results of the modified and reinforced concretes containing distinct steel fiber contents and associated with MGR and rubber particles additions, the follow conclusions can be drawn:

1. Distinct portions of the hooked-end steel fibers, rubber residues and marble and granite residues are successfully added to constituted reinforced concretes in order to attain substantial improvements in the damping results;
2. It is found that marble and granite residues additions have provided a high-density resulting microstructural array. The observed particles are much thinner than the aggregates and the voids are filled. Consequently, an increase of the paste density and the packaging of the particles associated with increasing in the mechanical properties is achieved;
3. It is corroborated that the marble and granite portions are used to minimize the loss of mechanical properties due to the incorporation of the rubber particles. The concrete with rubber residues have shown higher level of porosity than other ones. This has affected the transition zone and the mechanical behavior is decreased. On the other hand, a higher capacity to absorb energy and, consequently, higher damping factor than other examined samples is obtained. Additionally, it is also remarkable that not change the fact that the rubber content addition relatively worsens the compressive strength of concrete.
4. When designing a SCC mixture intending to improve the resulting damping ratio, associated with a compressive strength range between 70 and 75 MPa, the steel fiber addition has no demonstrated negative effects on the slump flow results. Although the rubber content has decreased the mechanical behavior and slump flow, the concatenated utilization of the MGR and hooked-end steel fiber can be considered in a SCC designing. This mainly in order to reach slight improvements in the damping results under certain acceptable compressive strength conditions. With this, the SCC/20SF/30MGR/5R sample seems to be a potential mixture, which also reveals a potential environmentally friendly aspect due to the decreasing trend of the cement consumption with incorporating marble is induced.
5. It is worth noting that in a construction project (e.g. flooring, underground or precast) there exist a great variety of distinctive other fiber types, e.g. flat end, undulated, hooked flat-end

 doi:10.20944/preprints202405.1143.v1

fiber and hooked glued fiber (ArcelorMittal®). The differences among these are geometry, dimensions and mainly its corresponding tensile strengths, i.e. 1100, 1500, 1200 and 2400 MPa, respectively. Based on this, it is clearly perceived that flat fibers (quasi conventional straight) have lower tensile strength than the hooked (~1350 MPa). This affects considerably the resulting mechanical properties, depending to desired construction type. Thus, the decision to adopt a conventional fiber or a hook or other type depends strongly to desire requirements, as well also the other additives utilized and demonstrated in this present investigation.

Author Contributions: A.E.G. and M.L.N.M. have elaborated mixtures and samples. L.A.G, M.L.N.M and R.C.C.L. have carried out the mechanical and microstructural characterizations, organized the data and correlated with attained results of all examined specimens. A.E.G. and W.R. O. have also helped empirical and theoretical correlations provided. Additionally, they have also contributed with the general organization and English writing. All authors have read and agreed to the published version of the manuscript.

Funding: The financial support provided by FAEPEX-UNICAMP (#2091/24), CAPES (Coordination for the Improvement of Higher Education Personnel), Ministry of Education, Brazil, Grant #1) and CNPq (The Brazilian Research Council) Grants, #310375/2020-7; #313272/2021-2; #310376/2020-3; 402704/2023-1, 407595/2022-8; #405602/2018-9 and FAPESP (São Paulo Research Foundation) Grants #2018/12076-5; #2018/14945-0.

Institutional Review Board Statement: Not applicable

Informed Consent Statement: Not applicable

Data Availability Statement: All research data supporting this publication are directly available within this publication.

Acknowledgments: Acknowledgments are also provided to Mr. Luiz Antonio Garcia (technician department) whom has contributed with technical aspects and equipment organization.

Conflicts of Interest: The authors declare no conflict of interest.

Abbreviations

ABNT NBR	*Associação Brasileira de Normas Técnicas*
NBR	Norma Brasileira Registrada
Al_2O_3	Aluminum oxide
ASTM	American Society for Testing and Materials
ATCP	Enterprise Physical Engineering
CH	Calcium hydroxide
C-S-H	Calcium silicate hydrate
CaO	Calcium oxide
CO_2	Carbon dioxide
CS	Compressive strength – (MPa)
E	Young's modulus– (GPa)
Ed	Dynamic Young's Modulus – (GPa)
Es	Estatic Young's Modulus – (GPa)
Fe_2O_3	Iron oxide or iron trioxide (or hematite)
HES	High early strength – Portland cement
HESF	Hooked-end steel fibers
IET	Impulse Excitation Technique – non-destructive method
J - ring	J ring method – Determination of passing ability – (mm)

 doi:10.20944/preprints202405.1143.v1

K_2O	Potassium oxide
MG	Marble/Granite
MgO	Magnesium oxide
MGR	Marble and Granite Residues
Na_2O	Sodium oxide
PJ	Passing ability
ISO	International Organization for Standardization
ITZ	Interfacial Transition Zone
R	Rubber – (kg/m³)
SE	Secondary electron
SEM	Secondary electron microscope
SCC	Self-compacting concrete
SF	Steel fiber – (kg/m³)
S_iO_2	Silicon dioxide
SP	Superplasticizer
TiO_2	Titanium dioxide
TS	Tensile strength – (MPa)
TZ	Transition Zone
T_{500}	Flow time in (s) for the concrete to achieve spreading within a 500 mm circle – (s)
VF (V Funnel)	Funnel for determining the viscosity of Self-Compacting Concrete
VS1 and VS2	Apparent Plastic Viscosity Classifications

List of Symbols

A	Amplitude corresponds to the first peak point (m)
A_n	Amplitude corresponds to the nth peak-point (n cycles later in the time)
δ	Logarithmic decrement
n	Corresponds to the nth peak (n cycles later in time history)
Z	Logarithmic decrement at time t = 0
$z(t)$	Response in logarithmic decrement time (s)
ζ	Damping ratio (dimensionless)
$\boldsymbol{\varrho}$	Specific mass of the concrete (kg/m³)
ω_0	Natural Frequency (Hz)
ω_d	Damped natural Frequency (Hz)

References

1. Okamura H, Ouchi M, Self-Compacting Concrete, J Adv Concr Technol 2003; 1: 5–15.
2. EFNARC, The European Guidelines for Self-Compacting Concrete - Specification, Production and Use, Eur Fed Spec Constr Chem Concr Syst 2005:63.
3. Topçu IB, Bilir T, Uygunoğlu T. Effect of waste marble dust contente as filler on properties of sel-compacting concrete. Constr Build Mater 2009; 23: 1947-1953.
4. Manikandan M, Felixkala T. Experimental study on properties of granite waste in self compacting concrete. Indian J Appl Res 2015; 5: 128-130.
5. Boukhelkhal, et al. Effects of marble powder as a partial replacement of cement on some engineering properties of self-compacting concrete, J Adhes Sci Technol 2016; 30: 2405-2419.

6. Sadek DM, El-Attar MM, Ali HA. Reusing of marble and granite powders in self-compacting concrete for sustainable development. J Clean Prod 2016; 121: 19-32.
7. Hameed A, et al. Self compacting concrete: use of waste marble powder as filler material. Pak J Engg & Appl Sci 2016; 18: 1-10.
8. Alyamac KE, Ghafari E, Ince R. Development of eco-efficient self-compacting concrete with waste marble powder using the response surface method. J Clean Prod 2017; 144: 192-202.
9. Tennich M, Ouezdou MB, Kallel A. Thermal effect of marble and tile fillers on self-compacting concrete behavior in the fresh state and at early age. J Build Eng 2018; 20: 1-7.
10. Choudhary R, Gupta R, Nagar R. Impact on fresh, mechanical, and microstructural properties of high strength self-compacting concrete by marble cutting slurry waste, fly ash, and silica fume. Constr Build Mater 2020; 239: 117888.
11. Alyousef, et al. Study of the effects of marble powder amount on the self-compacting concretes properties by microstructure analysis on cement-marble powder pastes. Adv Civ Eng 2018; 2018: ID 6018613.
12. Li N, et al. Properties of self-compacting concrete (SCC) with recycled tire rubber aggregate: A comprehensive study. J Clean Prod 2019; 236: 117707.
13. Si R, et al. Evaluation of laboratory performance of self-consolidating concrete with recycled tire rubber. J Clean Prod 2018; 180: 823-831.
14. Aslani F, et al. Experimental investigation into rubber granules and their effects on the fresh and hardened properties of self-compacting concrete. J Clean Prod 2018; 172: 1835-1847.
15. Sugapriya P, Ramkrishnan R. **Crumb rubber recycling in enhancing damping properties of concrete.** IOP Conference Series: Materials Science and Engineering 2018; 310: 012013.
16. Hilal NN. Hardened properties of self-compacting concrete with different crumb rubber size and contente. International Journal of Sustainable Built Environment 2017; 6: 191-206.
17. Meesit R, Kaewunruen S. **Vibration characteristics of micro-engineered crumb rubber concrete for railway sleeper applications.** J Adv Concr Technol 2017; 15: 55-66.
18. Moustafa A, Elgawady MA. Mechanical properties of high strength concrete with scrap tire rubber. Constr Build Mater 2015; 93: 249-256.
19. Yung WH, Yung LC, Hua LH. A study of the durability properties of waste tire rubber applied to self-compacting concrete. Constr Build Mater 2013; 41: 665-672.
20. Zheng L, Huo XS, Yuan Y. Experimental investigation on dynamic properties of rubberized concrete. Constr Build Mater 2008; 22: 939-947.
21. Ismail MK, Hassan AAA. Impact Resistance and Mechanical Properties of Self-Consolidating Rubberized Concrete Reinforced with Steel Fibers. J Mater Civ Eng 2017; 29: 04016193.
22. Poveda E, et al. Influence of the fiber content on the compressive low-cycle fatigue behavior of self-compacting SFRC. Int J Fatigue 2017; 101: 9-17.
23. Aslani F, Kelin J. Assessment and development of high-performance fibre-reinforced lightweight self-compacting concrete including recycled crumb rubber aggregates exposed to elevated temperatures. J Clean Prod 2018; 200: 1009-1025.
24. Ghasemi M, Ghasemi MR, Mousavi SR. Studying the fracture parameters and size effect of steel fiber-reinforced self-compacting concrete. Constr Build Mater 2019; 201: 447-460.
25. Gokulnath V, Ramesh B, Sivashankar S. Influence of M sand in self compacting concrete with addition of steel fiber. Materials Today: Proceedings 2020; 22: 1026-1030.
26. Eisa AS, Elshazli MT, Nawar MT. Experimental investigation on the effect of using crumb rubber and steel fibers on the structural behavior of reinforced concrete beams. Constr Build Mater 2020; 252: 119078.
27. Khodabakhshian A, Ghalehnovi M, Brito J, Shamsabadi EA. Durability performance of structural concrete containing silica fume and marble industry waste powder. J Clean Prod 2018; 170: 42-60.
28. Mashaly AO, El-Kaliouby BA, Shalaby BN, El – Gohary AM, Rashwan MA. Effects of marble sludge incorporation on the properties of cement composites and concrete paving blocks. J Clean Prod 2016; 112: 731-741.
29. Rana A, Kalla P, Csetenyi LJ. Sustainable use of marble slurry in concrete. J Clean Prod 2015; 94: 304-311.
30. Xavier BC, Verzegnassi E, Bortolozo AD, Alves SM, Lintz RCC, Gachet LA, Osório WR. Fresh and Hardened States of Distinctive Self-Compacting Concrete with Marble- and Phyllite-Powder Aggregate Contents. J Mater Civ Eng 2020; 32: 04020065.
31. Tomar AK, Gupta SK, Kumar A, Singh A. Review on Utilization of Waste Marble Powder in Self-Compacting Concrete. Int J Eng Trends Technol 2016; 37: 122-124.
32. Hammeed A, Qazi A, Abbas, Rehman A. Self-Compacting Concrete: Use of Waste Marble Powder as Filler Material. Pak. J. Engg. & Appl. Sci. 2016; 18: 1-10.
33. Tayeb B, Abdelbaki B, Madani , Mohamed L. Effect of Marble Powder on the Properties of Self-Compacting Sand Concrete. The Open Constr Build Technol J 2011; 5: 25-29.
34. Singh M, Choudhary K, Srivastava A, Singh Sangwan K, Bhunia D. A study on environmental and economic impacts of using waste marble powder in concrete. J Build Eng 2017; 13: 87–95.

35. Allam ME, Bakhoum ES, Garas GL. Re-use of granite sludge in producing green concrete. ARPN J Eng Appl Sci 2014; 9: 2731-2737.
36. Bušic R, Milicevic´I, Šipoš TK, Strukar K. Recycled Rubber as an Aggregate Replacement in Self-Compacting Concrete. Literature Overview. Mater 2018; 11: 1729.
37. Aslani F, Ma GW, Wan DLY, Muselin G. Development of high-performance self-compacting concrete using waste recycled concrete aggregates and rubber granules. J Clean Prod 2018; 182: 553-566.
38. Shu X., Huang B. **Recycling of waste tire rubber in asphalt and portland cement concrete: An overview.** Constr Build Mater 2014; 217-224.
39. Najim KB, Hall MR. Mechanical and dynamic properties of self-compacting crumb rubber modified concrete. Constr Build Mater 2012; 27: 521-530.
40. Athiyamaan V, Ganesh MG. Experimental, statistical and simulation analysis on impact of micro steel – Fibres in reinforced SCC containing admixtures. Constr Build Mater 2020; 246: 118450.
41. Suuronen J, Kallonen A, Eik M, Puttonen J, Serimaa R, Herrmann H. Analysis of short fibres orientation in steel fibre-reinforced concrete (SFRC) by X-ray tomography. J Mater Sci 2013; 48: 1358-1367.
42. Herrmann H, Pastorelli E, Kallonen A, Suuronen J. Methods for fibre orientation analysis of X-ray tomography images of steel fibre reinforced concrete (SFRC). J Mater Sci 2016; 51: 3772-3783.
43. Zhang S, Liao L, Song S, Zhang C. Experimental and analytical study of the fibre distribution in SFRC: a comparison between image processing and the inductive test. Compos Struct 2018; 188: 78-88.
44. Lee S-J, Hong Y, Eom A-H, Won J-P. Effect of steel fibres on fracture parameters of cementitious composites. Compos Struct 2018; 204: 658-63.
45. Heek P, Ahrens MA, Mark P. Incremental-iterative model for time-variant analysis of SFRC subjected to flexural fatigue. Mater Struct 2017; 50: 62.
46. Afroughsabet V, Biolzi L, Ozbakkaloglu T. High-performance fiber-reinforced concrete: a review. J Mater Sci 2016; 51: 6517-6551.
47. Cuenca E, Echegaray-Oviedo J, Serna P. Influence of concrete matrix and type of fiber on the shear behavior of self-compacting fiber reinforced concrete beams. Compos B Eng 2015; 75: 135-147.
48. Trindade YT, Bitencourt Jr LAG, Monte R, Figueiredo AD, Manzoli OL**. Design of SFRC members aided by a multiscale model: Part I – Predicting the post-cracking parameters.** Compos Struct 2020; 241: 112078.
49. Gomes PCC; Barros AR. Métodos de dosagem de concreto autoadensável, 1 ed. São Paulo: Pini; 2009.
50. Tutikian BF; Dal Molin D. Concreto Autoadensável, 2 ed. São Paulo: Pini; 2015.
51. Alberti MG, Enfedaque A, Gálvez JC. The effect of fibres in the rheology of self-compacting concrete. Constr Buil Mater 2019; 219: 144-153.
52. Ananda F, Febriani O, Pribadi JA, Junaidi G. Effect the used of steel fibers (Dramix) on reinforced concrete slab. J Infr Develop 2019; 2:183-191.
53. Clarence WS. Vibration Damping, Control, and Design. 1 ed. CRC Press; 2019.
54. Mehta K, Monteiro P. Concrete: Microstructure, Properties and Materials, 4 ed. São Paulo: IBRACON; 2014.
55. Neville, AM. Propriedades do concreto. 5 ed. Porto Alegre: Bookman; 2016.
56. BSI — BRITISH STANDARDS INSTITUTION. BS 8110-2:1985 - Structural use of concrete – Part 2: Code of practice for special circumstances. London, UK. 2001.
57. Lyndon, FD; Baladran, RV. Some observations on elastic properties of plain concrete, Cem Concr Res 1986; 16: 314-324.
58. Popovics, S. Verification of relationships between mechanical properties of concrete-like materials. Mat Constr 1975; 8: 183-191.
59. Haach VG, Carrazedo R, Oliveira LMF, Corrêa MRS. Application of acoustic tests to mechanical characterization of masonry mortars. NDT&E International 2013; 59: 18-24.
60. Rao, NSVK. Foundation Design: Theory and Practice. 1 ed., Wiley; 2011.
61. Angelin AF, Andrade MFF, Bonatti RS, Cecche Lintz RC, Gachet-Barbosa LA, Osório WR. Effects of spheroid and fiber-like waste-tire rubbers on interrelation of strength-to-porosity in rubberized cement and mortars. Constr Build Mater 2015; 95: 525-536.
62. Angelin AF, Cecche Lintz RC, Osório WR, Gachet LA. Evaluation of efficiency factor of a selfcompacting lightweight concrete with rubber and expanded clay contents. Constr Build Mater 2020; 257: 119573.
63. Aïtcin, PC. Concreto de Alto Desempenho. 1.ed., 667p, São Paulo: Pini, 2000.
64. Aslani F. Mechanical properties of waste tire rubber concrete mechanical properties of waste tire rubber concrete. J Mater Civ Eng 2016; 28: 04015152.
65. Angelin AF, Cecche Lintz RC, Barbosa LAG. Fresh and hardened properties of self-compacting concrete modified with lightweight and recycled aggregates. Rev IBRACON Estrut Mater 2018; 11: 76-94.
66. Duarte APC, Silva BA, Silvestre N, Brito J, Júlio E. Mechanical characterization of rubberized concrete using an image-processing/XFEM coupled procedure. Compos B Eng, 2015; 78: 214-226.
67. Pereira, A. H. A. et al. Algoritmo para determinação do amortecimento de materiais cerâmicos pela técnica das frequências naturais de vibração via excitação por impulso, Ceram 2012; 58: 229-237.

68. Otani LB, Pereira AHA. Estimation of the static modulus of elasticity of concrete using the impulse excitation technique. ATCP Phys Eng 2016; 38: 1-38.
69. Khatri RP, Sirivivatnanon V, Gross W. Effect of different supplementary cementitious materials on mechanical properties of high performance concrete. Cem Concr Res 1995; 25: 209-220.
70. Bachmann H et al. Vibration problems in structures: practical guidelines. 2 ed. Berlin: Birkhäuser Verlag; 1997.
71. Swamy SS, Sreedhar B, Kalas VJ, Chandan KM. Experimental studies on compression and vibration characteristics of granite epoxy- an alternative material for precision machine tool beds. IJPRET 2014; 2: 120-135.
72. Thakare AA, Siddique S, Sarode S N, Deewan R, Gupta V, Gupta S, Chaudhary S A study on rheological properties of rubber fiber dosed self-compacting mortar. Constr Build Mater 2020; 262: 120745.
73. Angelin AF, Miranda EJP, Dos Santos JMC, Lintz RCC; Gachet-Barbosa LA. Rubberized mortar: The influence of aggregate granulometry in mechanical resistances and acoustic behavior. Constr Build Mater 2019; 200: 248-254.
74. Silva FM; Miranda Jr EJP, Dos Santos JMC, Gachet-Barbosa LA, Gomes AE, Lintz RCC. The use of tire rubber in the production of high-performance concrete. Cerâm 2019; 65: 110-114.
75. Zhu H, Wang Z, Xua J, Han Q. Microporous structures and compressive strength of high-performance rubber concrete with internal curing agent. Constr Build Mater 2019; 215: 128-134.
76. Gupta T, Chaudhary S, Sharma RK. Assessment of mechanical and durability properties of concrete containing waste rubber tyre as fine aggregate. Constr Build Mater 2014; 73: 562-574.
77. Silva FM, Barbosa LAG, Lintz RCC, Jacintho AEPGA. Investigation on the properties of concrete tactile paving blocks made with recycled tire rubber. Constr Build Mater 2015; 91: 71-79.
78. Sridhar R, Prasad R. Vibration based damaged detection of steel fiber reinforced concrete. Materials Today: Proceeding 18 (2019) 3321-3329.
79. Kamde DK, Pillai RG. Corrosion initiation mechanisms and servisse life estimation of concrete systems with fusion-bonded-epoxy (FBE) coated steel exposed to chlorides. Constr. Build. Mater. 277 (2021) 122314.
80. Ming J, Shi JJ. Distribution of corrosion products at the steel-concrete interface: Influence of mil scale properties, reinforcing steel type and corrosion inducing method. Constr. Build. Mater. 299 (2019) 116854.